iScience

CellPress
OPEN ACCESS

Article

Cellular lipids regulate the conformational ensembles of the disordered intracellular loop 3 in β2-adrenergic receptor

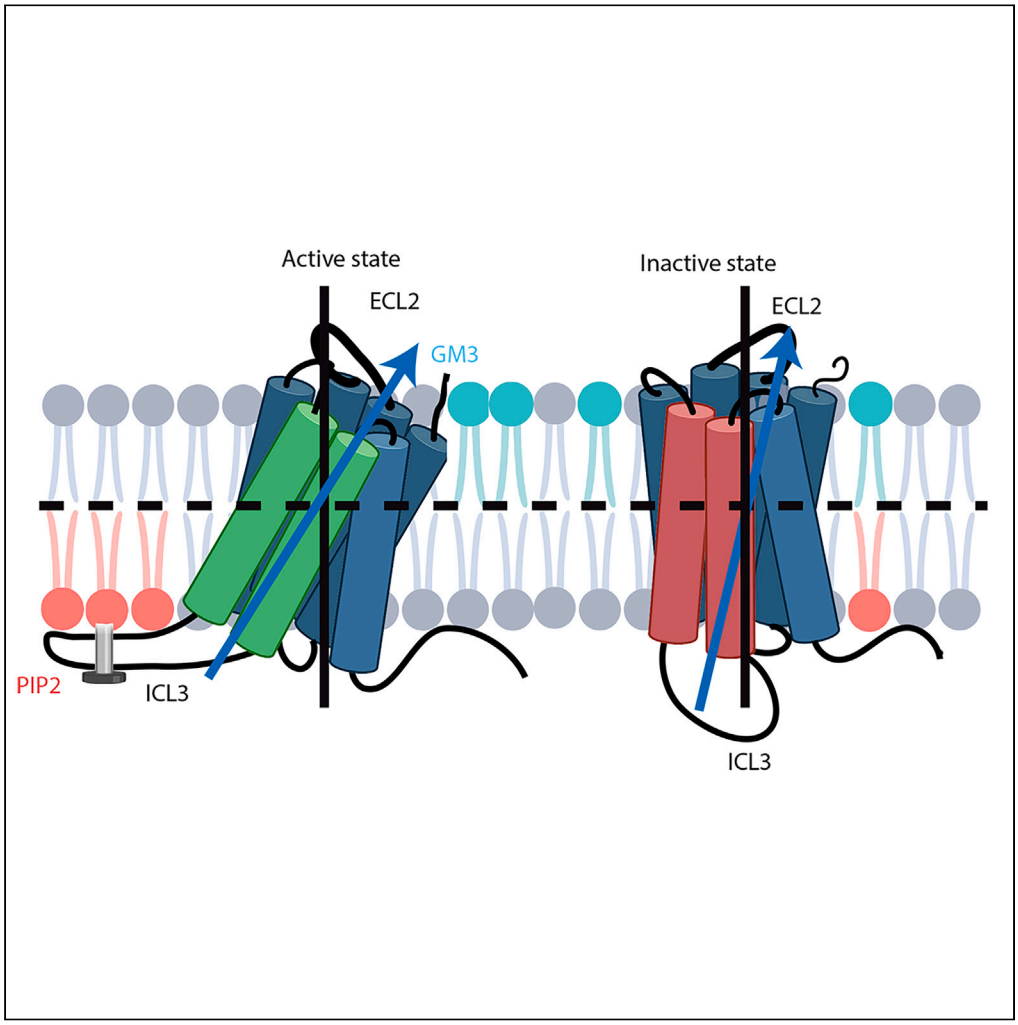

Elizaveta Mukhaleva, Tianyi Yang, Fredrik Sadler, Sivaraj Sivaramakrishnan, Ning Ma, Nagarajan Vaidehi

nma@coh.org (N.M.)
nvaidehi@coh.org (N.V.)

Highlights

Lipids in the cell membrane actively modulate the ICL3 conformations of GPCR

PIP2 specifically stabilizes the 3rd intracellular loop of β2AR in an open conformation

PIP2 interaction with the ICL3 enhances the active state of the receptor

Ganglioside GM3 gates the ligand allosterically in its binding site

Mukhaleva et al., iScience *27*, 110086
June 21, 2024
https://doi.org/10.1016/j.isci.2024.110086

iScience

CellPress
OPEN ACCESS

Article

Cellular lipids regulate the conformational ensembles of the disordered intracellular loop 3 in β2-adrenergic receptor

Elizaveta Mukhaleva,[1,2] Tianyi Yang,[1] Fredrik Sadler,[3,4] Sivaraj Sivaramakrishnan,[3,4] Ning Ma,[1,*] and Nagarajan Vaidehi[1,2,5,*]

SUMMARY

The intracellular loops of G protein-coupled receptors (GPCRs) have been shown to play a key role in G protein coupling and selectivity. We recently showed that the intrinsically disordered third intracellular loop (ICL3) of β2-adrenergic receptor is dynamic and equilibrates between open and closed conformations to regulate the G protein coupling. In this study, using the extensive molecular dynamics simulations in multi-lipid bilayer models, we show that the lipid phosphatidylinositol 4,5-bisphosphate (PIP2) stabilizes the active state of β2-adrenergic receptor by keeping ICL3 in an open conformation. This stabilization results in a tilt of the receptor within the membrane. Additionally, the ganglioside lipid, GM3 interacts with extracellular loops, impacting the ligand binding site allosterically. This demonstrates the active role of the chemistry of lipids in stabilizing specific GPCR conformations.

INTRODUCTION

The activity of G protein-coupled receptors (GPCRs) is often affected by the structures and chemistry of the lipid molecules that surround them in the membrane.[1] Both the types of lipids and relative composition of lipids in the bilayer influence the conformational ensemble of the receptor. Many studies have shown that different lipids play an important role in GPCR function.[2–9] NMR studies of β2-adrenergic receptor (β2AR) in detergent micelles compared to reconstituted high-density lipoprotein environment showed that the basal activity and exchange rates between inactive and active conformations are higher in detergents and in phospholipid bilayer containing high-density lipoprotein particles compared to cell membranes.[2,10,11] A study using mass spectrometry combined with computational methods on three class A GPCRs have shown that phosphatidylinositol 4,5-bisphosphate (PIP2) plays a critical role in the receptor activity.[6] Although it is known that cellular lipids have a definitive effect on receptor activity, the mechanism(s) by which cellular lipids affect the flexibility of the intra- and extracellular loops and thereby influence the receptor activity remains nebulous.

The three intracellular loops and the carboxy terminus of GPCRs play a critical role in coupling to G proteins and β-arrestins. The extracellular loops are also involved in not only regulating the ligand binding but also in G protein coupling.[12,13] However, receptor loop regions and N- and C termini are largely unstructured and often not resolved in the three-dimensional structures making it particularly difficult to study their role in GPCR function using structural techniques. Recent studies using biophysical techniques have shown that the intrinsically disordered intracellular loop 3 (ICL3) and the carboxy terminus of GPCRs regulate the receptor coupling selectivity to G proteins.[14,15] In our previous study[14] on β2AR, we found that ICL3 spans a broad ensemble of conformational states, ranging from "closed" states that block the binding site of the G protein to "open" states that allow for the G protein to bind.[14] Thus, ICL3 regulates the access to the G protein coupling site in the receptor. Through this mechanism, ICL3 acts as a secondary regulator of β2AR activation as well as plays an important role in the G protein coupling strength and selectivity. Although it is evident from this study that ICL3 regulates the activity and signaling specificity of β2AR, the role of the membrane lipids in stabilizing the conformation of ICL3 is not known. In this study, we have used extensive molecular dynamics (MD) simulations (22 μs) in multi-lipid bilayer model that mimics the plasma membrane to analyze the effects of different types of lipids on the conformational ensemble of ICL3 and thereby their effects on β2AR activation.

[1]Irell and Manella Graduate School of Biological Sciences, Beckman Research Institute of the City of Hope, Duarte, CA, USA
[2]Department of Computational and Quantitative Medicine, Beckman Research Institute of the City of Hope, Duarte, CA, USA
[3]Biochemistry, Molecular Biology and Biophysics Graduate Program, University of Minnesota, Minneapolis, MN, USA
[4]Department of Genetics, Cell Biology and Development, University of Minnesota, Minneapolis, MN, USA
[5]Lead contact
*Correspondence: nma@coh.org (N.M.), nvaidehi@coh.org (N.V.)
https://doi.org/10.1016/j.isci.2024.110086

RESULTS

ICL3 acts as a secondary regulator β2AR of activity by forming a cap in the G protein binding site

As detailed in Table S1, we previously performed 22 μs of all-atom MD simulations on β2AR with agonist including the full-length ICL3 in various starting conformations in a multi-lipid bilayer comprising lipids consisting of POPC, DOPC, POPE, DOPE, POPS, DOPS, sphingomyelin (Sph), ganglioside (GM3), and cholesterol and PIP2.[14,16] We observed that ICL3 spanned a broad conformational ensemble in these simulations, with transitions between closed and open ensemble of conformations. The closed state of ICL3 is defined as a state where the C terminus of the ICL3 blocks the entry of α helix in the C terminus of the G protein. To enrich the conformations near the transition of closed to open state of ICL3, we performed a swarm of MD simulations by initiating simulations from multiple population density maxima along the transition pathway. The total MD simulation trajectories sum up to 22 μs long. We sought to further analyze the role of the lipid components in stabilizing the different conformational states of ICL3 thereby regulating the activity of β2AR.

We performed principal component analysis using the backbone atom coordinates of β2AR and projected the MD snapshots on the top two scoring principal components (PCs) (Figure 1A). Each maximum on the PC landscape represents a potential representative state of the system, capturing key conformational states within the trajectory. Next, we clustered the MD frames using their first two PCs (see STAR Methods) and obtained 12 distinct conformation clusters as depicted in Figures S1A–S1D. By overlapping Figure 1A with Figure S1C, it became apparent that 10 out of 12 clusters from Figure S1C corresponded with local maxima on the population density landscape in Figure 1A. Therefore, we focused our attention on those 10 clusters. We selected the ensemble of conformations around the 10 maxima for further analysis (see STAR Methods).

To establish the link between the functional (inactive, intermediate and active) states of β2AR and the loop conformation in the ten conformational clusters, we analyzed the distance between transmembrane (TM) helix 3, TM3-TM6 distance (3.50–6.34) that typifies the active state of β2AR,[17] and the positioning of residues R259 to L266 in ICL3 relative to the C-terminal end of TM7 (R328). In our prior research, we identified that this set of residues in ICL3 formed a turn and half of a helix and covered the G protein binding site as a loose "cap" (Figure 1B). This cap motif has two distinct conformations: one that obstructs the G protein binding site, while the other one is open (shown in Figure 1B, blue and green structure, respectively). The intracellular region of TM6 moves away from the intracellular region of TM3 upon activation of β2AR and this distance is used to assess the level activation of β2AR. Using these two metrics, we classified the ten conformational clusters as follows.

- The active state, in which the ICL3 cap is extended out of the G protein binding site and the entire ICL3 is in an open state, and the TM6 is away from TM3.
- The intermediate state, wherein TM6 remains away from TM3 but the ICL3 cap is loosely bound to the G protein coupling site.
- The inactive state, where TM6 is close to TM3 effectively occluding the G protein binding site. While the ICL3 cap is extended similarly to the active state, other portions of ICL3 stabilize the inactive state of the receptor through contacts with ICL2 and ICL1 residues.The fact that ICL3 contacts ICL1/ICL2 residues in the active state blocking the entry to the G protein and is bound to the G protein binding site in the intermediate state, suggests that ICL3 is a secondary regulator to the G protein entry.

To sort the 10 clusters into these three main conformational states of β2AR described previously, we used hierarchical clustering based on two parameters: the distance between residues 3.50 and 6.34, which reflects the TM3-TM6 distance, and the shortest distance between the ICL3 cap's residues (R259 to L266) and R328 on the TM7 (Figure 1C).The minimum distance between ICL3 cap residues and R328 distinctly differentiates intermediate states from active states with no overlap, leading us to select this as the metric to characterize the movement of the ICL3 cap. The hierarchical clustering identified three distinct clusters (Figure 1D). The first cluster exhibits a small 3.50–6.34 distance and a medium ICL3-TM7 distance. Upon visualization, this conformation closely aligns with the fully inactive state electron microscopy structure,[18] leading us to label this cluster as the "inactive state ensemble" (Figures 1B and 1C). The second cluster, with a large 3.50–6.34 distance and a small ICL3-TM7 distance, suggests that while the TM6 has shifted outward, the ICL3 cap still obstructs the G protein binding site (Figures 1B and 1C). We designate this as the "intermediate state ensemble." The third cluster shows a large 3.50–6.34 distance and a large ICL3-TM7 distance, indicating that the TM6 has swung out and the ICL3 cap is out of the G protein coupling site, and this is the active state ensemble (Figures 1B and 1C). To check if the separation of the conformation states also aligns with other microswitches known for class A GPCRs,[16,19,20] we calculated the changes in distances between R131$^{3.50}$-L272$^{6.34}$, Y219$^{5.58}$-Y326$^{7.53}$, and S207$^{5.46}$-I314$^{7.41}$ referred to as TM5 bulge. The distribution of these distances, including the TM5 bulge, does show clear separation between the active and inactive state ensembles in our study (Figures S1E–S1G). Here after in the manuscript, we will refer to these three states.

PIP2 stabilizes the ICL3 in an open conformation in the active state ensemble

The multi-lipid bilayer model has an assortment of lipids that are unevenly dispersed between its upper and inner leaflets.[6,7,16,19–22] We calculated the radial distribution function of the different lipids from the center of mass (CoM) of the receptor The simulation data indicate that the negatively charged lipid PIP2 displays higher concentrations close in proximity to β2AR (Figure S2A) Notably, PIP2 is only present in the intracellular side. Furthermore, the number of PIP2 molecules close to the receptor is far higher in the active state compared to the inactive state (Figure S2B). As PIP2 has been previously shown to influence membrane receptor activity,[6,7,16,21–24] we further investigated the influence of PIP2 on the conformation of ICL3.

Initially, we examined the role of PIP2 in stabilizing different conformations of ICL3. We identified the PIP2 molecules that form persistent contact (>20% simulation time) with residues on the IC loops, then we projected the CoM of these PIP2 molecules and the seven TM helices on

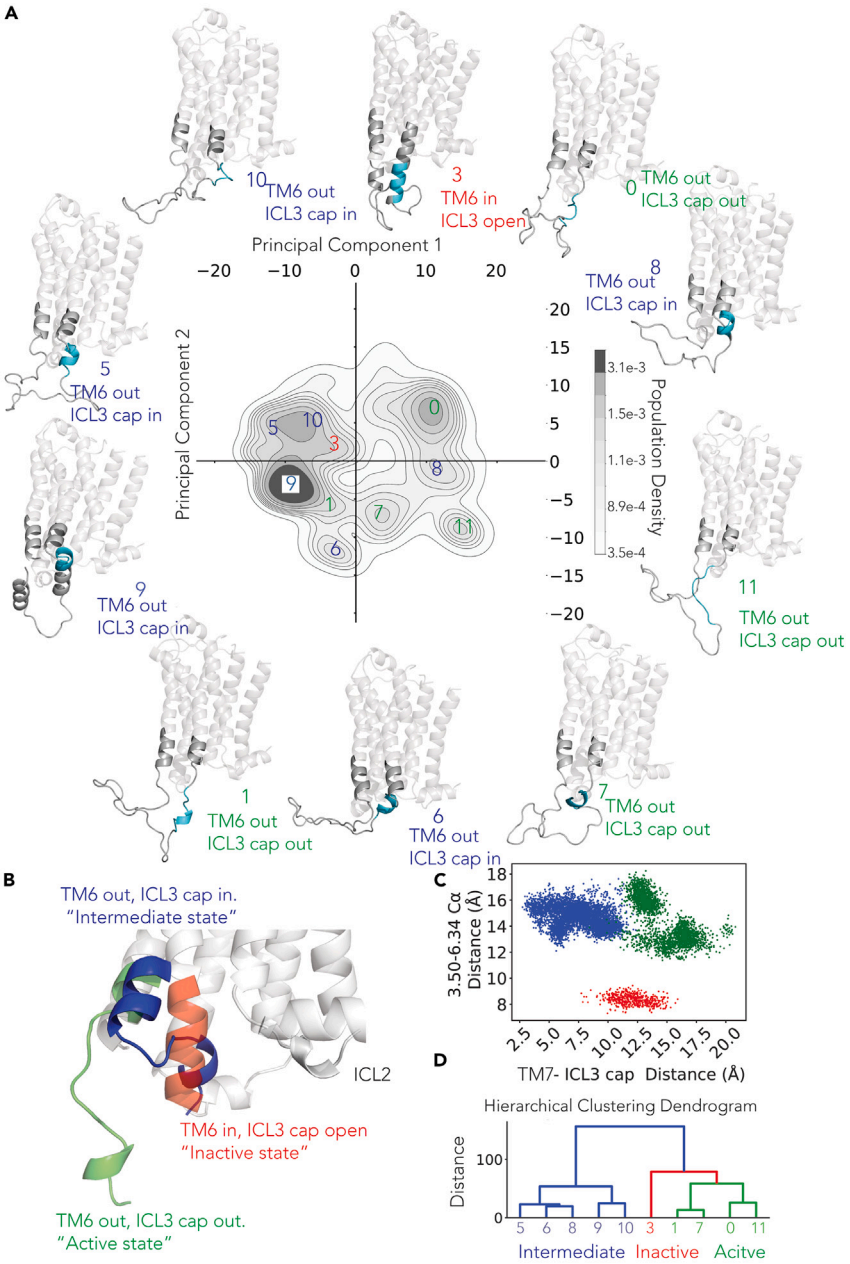

Figure 1. ICL3 acts as a secondary regulator of β2AR activity

(A) Population density landscape showing the conformational ensembles of β2AR-ICL3. The population density landscape is shown in the principal component space (PC1 and PC2). The representative structures (colored gray) of the 10 distinct conformational clusters are shown. The ICL3 region is colored in dark gray, the ICL3 cap is colored in cyan. The conformational clusters of the active states are labeled in green, the intermediate states are labeled in blue, and the inactive states are labeled in red.

(B) Structure overlay to show the positions of TM6 and ICL3 in the inactive (red) intermediate (blue) and active (green). In the inactive state structure (red), TM6 is close to TM3 blocking the G protein binding site, and the ICL3 cap is open and making contacts with ICL2 and ICL1 residues. In the intermediate structure (blue), TM6 has moved outward, ICL3 cap partially obstructs the G protein binding site. Both TM6 and ICL3 cap are out in the active state (green). Only the cap region of ICL3 is shown for clarity.

(C) Projection of all MD snapshots using the 3.50 and 6.34 distance and ICL3 cap-TM7 distance.

(D) The hierarchical clustering dendrogram of the ten clusters, using 3.50–6.34 distance and ICL3 cap-TM7 distance to separate the ten clusters into three major states.

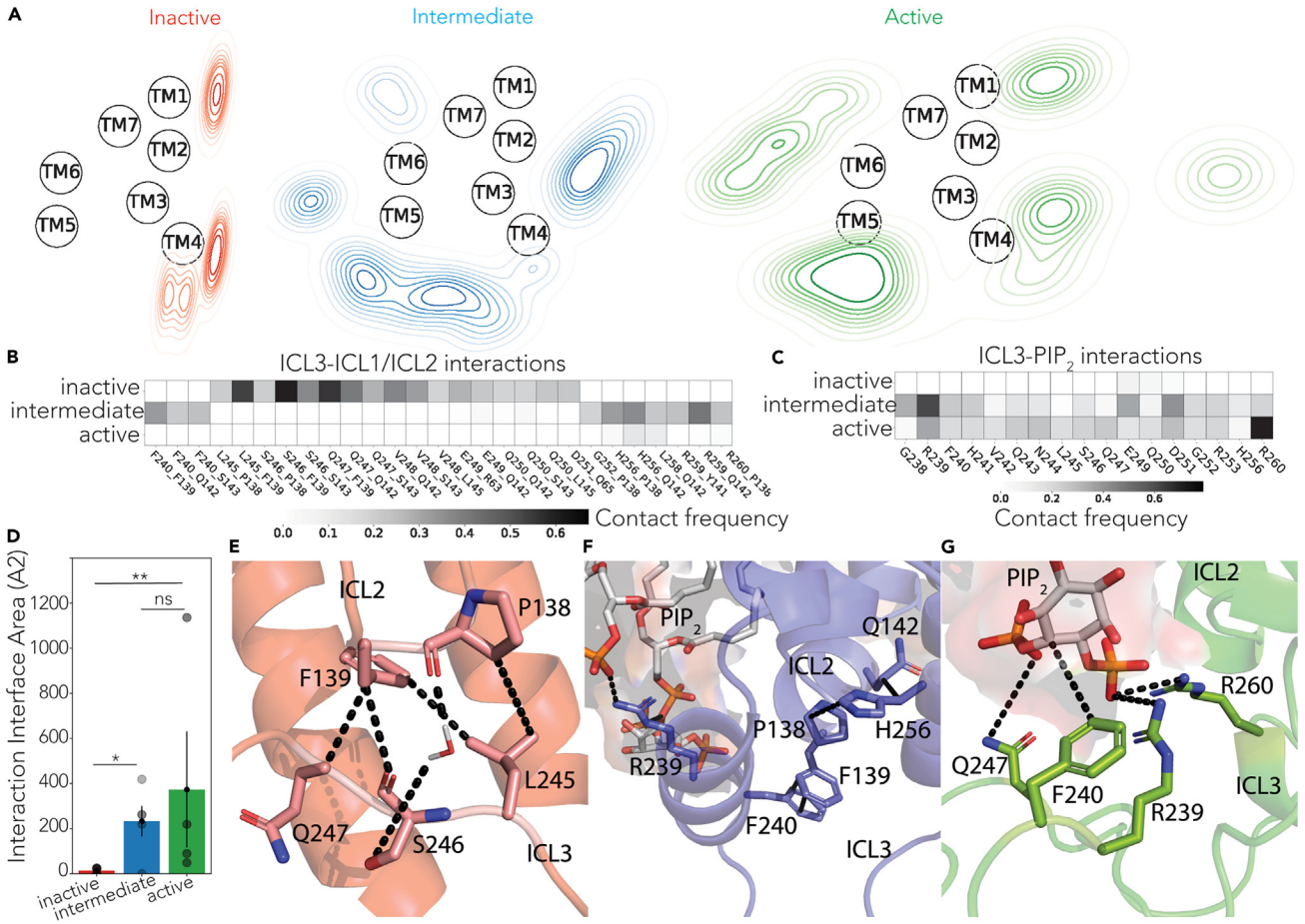

Figure 2. PIP2 competes with ICL1/2 for ICL3 binding and facilitates β2AR activation

(A) Density of PIP2 distribution surrounding the seven-transmembrane domain for the three prime states. The contour visualization is derived by projecting the center of mass (CoM) of the PIP2 head group onto the XY plane of the simulation box, with subsequent density calculations based on a defined grid. Red/Blue/Green contour map refers to the population density of PIP2 near the receptor in inactive/intermediate/active states. The CoM of ICL1/ICL2 residues and the center of mass of the middle of ICL3 (residue 250) is also projected on the XY plane.

(B) Frequency heatmap of the contacts between ICL3 and ICL1/2 residues.

(C) Frequency heatmap of the contacts between ICL3 residues and any PIP2 molecules.

(D) The interaction interface area between ICL3 and all the lipids that show contact persistence (>20%) with ICL3 residues. The ICL3-lipid interface area was calculated as the average value of all the 10 clusters for each of the conformational states. *p* value for significance: ns – $p = 0.722$, * - $p = 0.0278$, ** - $p = 0.0079$.

(E–G) The representative structure of ICL3 conformations in inactive/intermediate/active states, respectively, highlighting some of the residue contacts between ICL3-ICL1/2 or ICL3-PIP2.

to the X-Y plane of the membrane as population density contour map. As shown in Figure 2A, there is an increased density of PIP2 near the TM5/TM6/ICL3 region in both active and intermediate states. In the inactive states, PIP2 is found near the TM2/TM4/ICL1/ICL2 region. The PIP2 high-density regions identified from our MD are in line with previous study on A_{2A}R/NTSR1/β1AR.[6,7,25] A study that combined mass spectrometry with PIP2 binding on neurotensin receptor 1 showed that mutation of a set of four residues on TM4 affects the PIP2 binding the most, followed by mutation of three residues on TM1.[6] We calculated the frequency of contact of the corresponding residues on TM4 and TM1 in β2AR with PIP2. In agreement with the experimental study, we observed that the basic residues on TM4 show a higher contact frequency in the active state ensemble than the basic residues on TM1 (see Table S3).

We calculated the interaction between PIP2 and ICL3, and the interactions of ICL3 with the other two IC loops, ICL1 and ICL2. In the inactive state of β2AR, there is a significant number of contacts between residues in ICL3 and ICL2 with more than 20% frequency (Figure 2B), but no interaction between ICL3 and PIP2 (Figure 2C). In the fully active state, ICL3 residues show persistent interactions with PIP2 (Figure 2C) and decreased interactions with ICL2 and ICL1 (Figure 2B). In the intermediate state ensemble, there is an increase in the number of persistent contacts between ICL3 and PIP2 (Figure 2C) compared to the inactive state and a concurrent decrease in interactions between ICL3 and both ICL1 and ICL2 (Figure 2B). Thus, the interplay between contacts of ICL1/ICL2 and PIP2 with ICL3 plays a pivotal role in stabilizing different conformational states of β2AR.

We hypothesized that as ICL3 interacts favorably with PIP2, it will act as an anchor within the cell membrane, embedding the receptor deeper into the membrane bilayer. Supporting this, the contact surface area between ICL3 residues and all types of lipids is significantly higher in the active state than in the inactive state (Figure 2D).

The exchange between interloop contacts and ICL3-PIP2 contacts accounts for this discrepancy (Figures 2E–2G). In the inactive state ensemble, F139 from ICL2 interacts with multiple residues L245, S246, and Q247 from ICL3 (Figure 2E), forming a hydrophobic patch that covers the G protein binding site. There are also sporadic contacts (roughly 27.5% of the simulation time) between E249/D251 of ICL3 and R63/Q65 of ICL1. In the intermediate states, the contacts between L245, S246, and Q247 weaken. Instead, ICL3 residues F240, H256, and R259 interact with ICL2 residues F139 and Q142. In the active state ensemble, there are no significant contacts between ICL3 and ICL1/2; the only less persistent pairs (<20% simulation time) are between H256 and L258 in ICL3 and Q142 in ICL2. While majority of the ICL3-ICL1/ICL2 contacts are hydrophobic in nature, the contacts between ICL3 and PIP2 are polar. In both active and intermediate states, the R239 and R260 form stable contacts with the negatively charged PIP2 head group (Figures 2F and 2G). These ionic interactions anchor ICL3 in the membrane. Based on these results, we hypothesize that a competition exists between PIP2 and ICL1/2 for ICL3 interaction. When ICL3 binds with ICL1 and/or ICL2, it tends to favor more inactive states, whereas binding with PIP2 stabilizes active state ensemble. Both the contact frequency between ICL3 residues with PIP2 and the corresponding interaction energies (Figure S2C) show that PIP2 stabilizes the open conformation of ICL3 (in the active state) relative to the closed conformation (in the inactive state). Although we cannot conclude from these findings that PIP2 causes the transition of ICL3 between closed and open states, it is evident that PIP2 stabilizes the active state ensemble, thereby indirectly influencing the receptor activity.

To verify if other negatively charged lipids (POPS and DOPS) in our model of the cell membrane have a stabilizing effect on β2AR, we calculated the contact frequency of POPS and DOPS with the ICL3 residues in the active state ensemble. These lipids did not show a significant contact frequency with ICL3 residues compared to PIP2 (Figures S2D and S2E).

PIP2 interaction with ICL3 in the membrane bilayer tilts β2AR thus increasing the interaction interface of the receptor with the lipids

As described in the previous section, there is tight anchoring of ICL3 to PIP2 in the multi-lipid bilayer in the active state ensemble. This prompted us to study the effect of these anchoring interactions on the orientation of the receptor within the bilayer. To quantify this, we used the plane going across the middle of the lipid bilayer and computed the angle between the principal axis of β2AR and this plane (Figure 3A). As shown in Figure 3A, the distribution of the tilt angle for various receptor states shows that both active and intermediate states have a pronounced tilt angle and a broad distribution of tilt angles in comparison to the inactive state ensemble. One possibility is that the observed tilt of the receptor could be a consequence of variations in membrane thickness and hydrophobic mismatch. To clarify this, we calculated the membrane thickness across the three functional states that show little variation (ranging from 41.7 to 42.6 Å $\pm$ 1 Å) (Figure 3B). The two lipids GM3 and PIP2 that accumulate close to the receptor (Figure S2A) do not show much variation in acyl tail length (Table S4). Taken together, these data show that the tilt of β2AR in the active state is likely due to its favorable interaction with PIP2.

We studied the effect of the tilting motion seen in the active state of β2AR on the agonist binding site located in the extracellular region of β2AR. We analyzed the flexibility of the agonist, P0G (8-[(1R)-2-{[1,1-dimethyl-2-(2-methylphenyl)ethyl]amino}-1-hydroxyethyl]-5-hydroxy-2H-1,4-benzoxazin-3(4H)-one), in its binding site in the inactive, active, and intermediate states. We calculated root-mean-square deviation (RMSD) in coordinates of the ligand over the entire MD ensemble as shown in Figure 3C. The distribution of RMSD reveals that the agonist is less flexible in the active state ensemble (mean RMSD = 0.75 Å) compared to the inactive state ensemble (mean RMSD = 1.2 Å). Furthermore, we observed that the increased flexibility of the agonist in the inactive state comes from movement of the extracellular loops ECL2 and ECL3. Residues D192 in ECL2 and K305 in ECL3 form the salt bridge known to be important for ligand binding.[26] The distance between these residues increases in the inactive state (5.1 Å) compared to the active state (3.2 Å), presumably weakening this salt bridge and increasing structural flexibility within the ECL2-ECL3 domain (Figure 3D).

Our previous study demonstrated that the Ganglioside lipid (GM3) influences the dynamics of the extracellular loops of GPCRs.[16] This prompted us to study the interaction of GM3 with the extracellular loops. As shown in Figure S3, the density of GM3 projected on the XY plane of the membrane is high around the ECL2/ECL3 regions of β2AR in all the three states. Notably, the elongated sugar chain head of GM3 appears to flex, potentially covering the ECL2 region (Figure 3E). By analyzing the contact frequency between residues in ECL2 and ECL3 and GM3, we identified that residues R175, E188, N301, and L302 show consistent contact with GM3 across all three states (Figure 3F). However, a greater number of residues (12 residues) make persistent contacts (>50% of the MD simulation snapshots) with GM3 in the active states compared to the inactive states (6 residues). Thus, GM3 could play an important role in holding the ligand in place in the receptor.

DISCUSSION

In this study, we provide mechanistic evidence for the influence of lipid composition on the activity of β2AR predominantly through the ICL3 region of the receptor. This study supports previous findings concerning the influence of ICL3 on receptor activation through its broad conformational ensemble. We further delineated an important structural element of this ensemble, a short helical turn in the C terminus of ICL3 that caps the G protein binding site. This "cap" forms when the receptor displays other structural hallmarks of activation (TM3-TM6 distance), indicating that ICL3 is a secondary regulator of the activation of β2AR. As shown in Figure 4, we have shown that the negatively charged lipid, PIP2 interacts favorably with the ICL3 residues in the active state ensemble of the receptor, thus opening up the ICL3 for G protein signaling. This

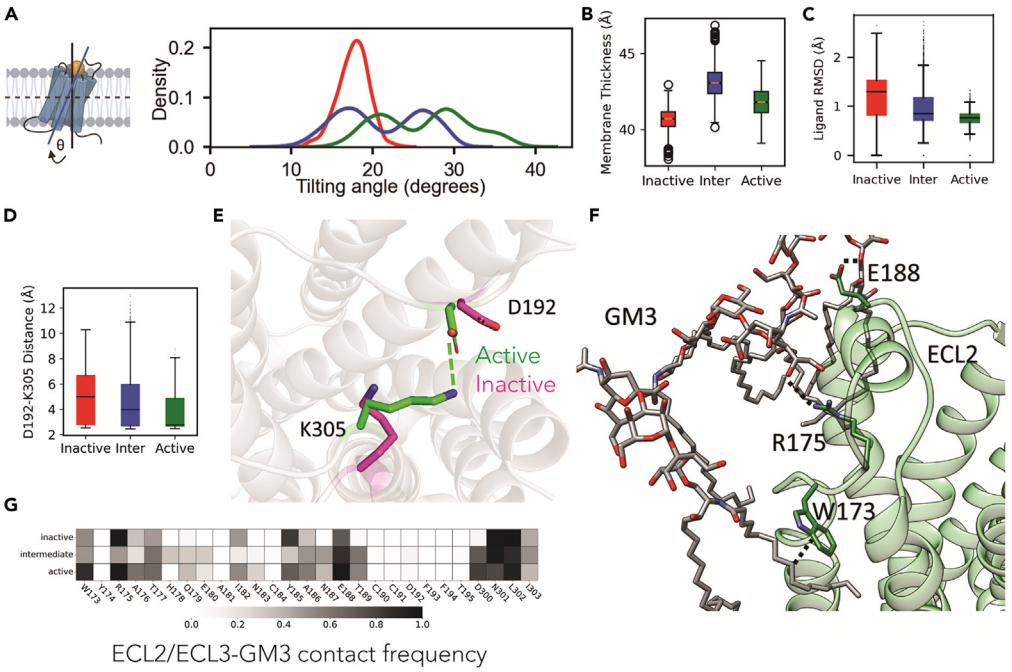

Figure 3. ICL3 anchoring in membrane leads to β2AR tilting, exerting an allosteric effect on the ligand binding pocket

(A) Tilting angle (θ) of GPCR in membrane for the inactive, intermediate, and active states.

(B) The membrane thickness in the inactive, intermediate, and active MD trajectories. The horizontal bar in the middle of each box represents the median value. The box itself represents the interquartile range (IQR), encompassing the first quartile to the third quartile. The whiskers extend to ± 1.5 IQR, representing the range of the data excluding outlies. The raw data points is shown as circle. The same applies to panels C and D. Significance is tested by ANOVA, $p < 0.0001$ for any two groups.

(C) Root-mean-square deviation (RMSD) of the coordinates of the agonist atoms in the inactive, intermediate, and active MD trajectories. Significance is tested by ANOVA, $p < 0.0001$ for any two groups.

(D) The minimum distance between D192 (ECL2) and K305 (ECL3) residue salt bridge in the inactive, intermediate, and active state MD trajectories. Significance is tested by ANOVA, $p < 0.001$ for any two goups.

(E) Three-dimensional structural representations highlighting the positions of D192 and K305. These amino acid residues are instrumental in maintaining the closed conformation between ECL2 and ECL3 regions.

(F) Three-dimensional structural representation of the interaction between GM3 molecule and ECL2 residues.

(G) Contact heatmap between GM3 and ECL2/ECL3 residues.

agrees with previous findings that PIP2 is known to stabilize GPCR-G protein complex formation.[6,7,16] Sequence alignment of β2AR with GPCRs of similar ICL3 lengths reveals a degree of sequence similarity in both ICL2 and ICL3 regions (see Figure S4). This similarity suggests that the competitive interaction observed between ICL2 and PIP2 for ICL3 may also be present in other GPCRs.

This PIP2-ICL3 anchor exerts an allosteric effect on the receptor through tilting of the receptor in the plasma membrane, stabilization of extracellular loop conformation, and ultimately stabilization of agonist binding. This stabilization is further coordinated by interactions

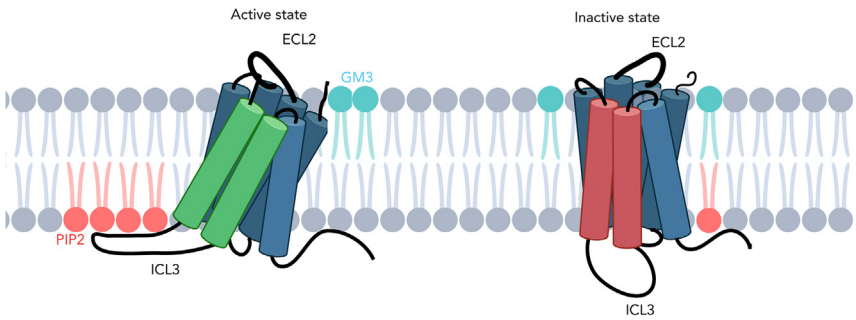

Figure 4. PIP2 anchors the active state of β2AR in the bilayer leading to stabilization of the open state of ICL3

This results in tilting of the receptor. GM3 on the outer leaflet of the membrane interacts strongly with ECL2 in membrane facilitating β2AR tilting, which further constrains the ligand binding site.

between ECL2 and GM3, a lipid which is predominantly in the upper leaflet of the membrane[6,7,16] and is known to regulate GPCR conformational dynamics.[16,27] Our latest findings reinforce the assertion that lipids are integral to GPCR dynamics. In summary, our study provides deep mechanistic insight into the role of lipids and therefore the role of cell membrane components in the regulation of receptor activity by intrinsically disordered loop regions in GPCRs.

Limitations of the study

We acknowledge that the 22 μs of MD simulations may not fully sample the conformational space of the disordered ICL3 regions. The prediction of the role of the lipids on GPCR activity needs to be validated experimentally.

STAR★METHODS

Detailed methods are provided in the online version of this paper and include the following:

- KEY RESOURCES TABLE
- RESOURCE AVAILABILITY
  - Lead contact
  - Materials availability
  - Data and code availability
- METHOD DETAILS
  - MD simulations trajectories preparation
  - Principal component analysis on GPCR backbone and acquire sub cluster trajectories
  - Distance measurement and hierarchical clustering
  - Contact analysis
  - Projecting lipid/GPCR onto X-Y plane
  - Interaction interface area calculation
  - Calculation of membrane thickness
  - Radial pair distribution function G(r) calculation
  - Ligand RMSD calculation
- QUANTIFICATION AND STATISTICAL ANALYSIS

SUPPLEMENTAL INFORMATION

Supplemental information can be found online at https://doi.org/10.1016/j.isci.2024.110086.

ACKNOWLEDGMENTS

This research was funded by the NIH (R01-GM117923 to N.V., R35-GM126940 to S.S., and T32-AR007612 to F.S.).

AUTHOR CONTRIBUTIONS

N.V. initiated the ideas. N.M. designed the data analysis strategies. E.M., T.Y., and N.M. performed the data analysis. N.M., F.S., S.S., and N.V. wrote the manuscript, and N.V. edited the manuscript extensively. N.V. performed project administration and funding acquisition.

DECLARATION OF INTERESTS

S.S. is a coinventor on the US patent "Cell Free Detection Of Intrinsic Efficacy of G Protein-Coupled Receptor Ligands" that uses giant plasma membrane vesicle-derived GPCR biosensors to probe ligand efficacy for G protein signaling pathways.

DECLARATION OF GENERATIVE AI AND AI-ASSISTED TECHNOLOGIES IN THE WRITING PROCESS

A few sentences written by one of the authors were submitted to ChatGPT to sharpen the sentence. However, the whole manuscript was subsequently edited extensively by the senior author and hence the use of ChatGPT became irrelevant. The authors take full responsibility for the content of the publication.

Received: November 16, 2023
Revised: March 19, 2024
Accepted: May 20, 2024
Published: May 23, 2024

REFERENCES

1. Lee, A.G. (2004). How lipids affect the activities of integral membrane proteins. Biochim. Biophys. Acta *1666*, 62–87. https://doi.org/10.1016/j.bbamem.2004.05.012.
2. Staus, D.P., Wingler, L.M., Pichugin, D., Prosser, R.S., and Lefkowitz, R.J. (2019). Detergent- and phospholipid-based reconstitution systems have differential effects on constitutive activity of G-protein–coupled receptors. J. Biol. Chem. *294*, 13218–13223. https://doi.org/10.1074/jbc.AC119.009848.
3. Dijkman, P.M., and Watts, A. (2015). Lipid modulation of early G protein-coupled receptor signalling events. Biochim. Biophys. Acta *1848*, 2889–2897. https://doi.org/10.1016/j.bbamem.2015.08.004.
4. Dawaliby, R., Trubbia, C., Delporte, C., Masureel, M., Van Antwerpen, P., Kobilka, B.K., and Govaerts, C. (2016). Allosteric regulation of G protein–coupled receptor activity by phospholipids. Nat. Chem. Biol. *12*, 35–39. https://doi.org/10.1038/nchembio.1960.
5. Sengupta, D., Prasanna, X., Mohole, M., and Chattopadhyay, A. (2018). Exploring GPCR–Lipid Interactions by Molecular Dynamics Simulations: Excitements, Challenges, and the Way Forward. J. Phys. Chem. B *122*, 5727–5737. https://doi.org/10.1021/acs.jpcb.8b01657.
6. Yen, H.-Y., Hoi, K.K., Liko, I., Hedger, G., Horrell, M.R., Song, W., Wu, D., Heine, P., Warne, T., Lee, Y., et al. (2018). PtdIns(4,5)P2 stabilizes active states of GPCRs and enhances selectivity of G-protein coupling. Nature *559*, 423–427. https://doi.org/10.1038/s41586-018-0325-6.
7. Song, W., Yen, H.Y., Robinson, C.V., and Sansom, M.S.P. (2019). State-dependent Lipid Interactions with the A2a Receptor Revealed by MD Simulations Using In Vivo-Mimetic Membranes. Structure *27*, 392–403.e3. https://doi.org/10.1016/j.str.2018.10.024.
8. Sejdiu, B.I., and Tieleman, D.P. (2020). Lipid-Protein Interactions Are a Unique Property and Defining Feature of G Protein-Coupled Receptors. Biophys. J. *118*, 1887–1900. https://doi.org/10.1016/j.bpj.2020.03.008.
9. Ueda, T., Kofuku, Y., Okude, J., Imai, S., Shiraishi, Y., and Shimada, I. (2019). Function-related conformational dynamics of G protein–coupled receptors revealed by NMR. Biophys. Rev. *11*, 409–418. https://doi.org/10.1007/s12551-019-00539-w.
10. Tsukamoto, H., and Farrens, D.L. (2013). A Constitutively Activating Mutation Alters the Dynamics and Energetics of a Key Conformational Change in a Ligand-free G Protein-coupled Receptor. J. Biol. Chem. *288*, 28207–28216. https://doi.org/10.1074/jbc.M113.472464.
11. Kofuku, Y., Ueda, T., Okude, J., Shiraishi, Y., Kondo, K., Mizumura, T., Suzuki, S., and Shimada, I. (2014). Functional Dynamics of Deuterated β 2 -Adrenergic Receptor in Lipid Bilayers Revealed by NMR Spectroscopy. Angew. Chem. Int. Ed. Engl. *53*, 13376–13379. https://doi.org/10.1002/anie.201406603.
12. DeVree, B.T., Mahoney, J.P., Vélez-Ruiz, G.A., Rasmussen, S.G.F., Kuszak, A.J., Edwald, E., Fung, J.J., Manglik, A., Masureel, M., Du, Y., et al. (2016). Allosteric coupling from G protein to the agonist-binding pocket in GPCRs. Nature *535*, 182–186. https://doi.org/10.1038/nature18324.
13. Lee, S., Nivedha, A.K., Tate, C.G., and Vaidehi, N. (2019). Dynamic Role of the G Protein in Stabilizing the Active State of the Adenosine A2A Receptor. Structure *27*, 703–712.e3. https://doi.org/10.1016/j.str.2018.12.007.
14. Sadler, F., Ma, N., Ritt, M., Sharma, Y., Vaidehi, N., and Sivaramakrishnan, S. (2023). Autoregulation of GPCR signalling through the third intracellular loop. Nature *615*, 734–741. https://doi.org/10.1038/s41586-023-05789-z.
15. Heng, J., Hu, Y., Pérez-Hernández, G., Inoue, A., Zhao, J., Ma, X., Sun, X., Kawakami, K., Ikuta, T., Ding, J., et al. (2023). Function and dynamics of the intrinsically disordered carboxyl terminus of β2 adrenergic receptor. Nat. Commun. *14*, 2005. https://doi.org/10.1038/s41467-023-37233-1.
16. Ma, N., Lee, S., and Vaidehi, N. (2020). Activation Microswitches in Adenosine Receptor A 2A Function as Rheostats in the Cell Membrane. Biochemistry *59*, 4059–4071. https://doi.org/10.1021/acs.biochem.0c00626.
17. Dror, R.O., Arlow, D.H., Borhani, D.W., Jensen, M.Ø., Piana, S., and Shaw, D.E. (2009). Identification of two distinct inactive conformations of the beta2-adrenergic receptor reconciles structural and biochemical observations. Proc. Natl. Acad. Sci. USA *106*, 4689–4694. https://doi.org/10.1073/pnas.0811065106.
18. Altenbach, C., Kusnetzow, A.K., Ernst, O.P., Hofmann, K.P., and Hubbell, W.L. (2008). High-resolution distance mapping in rhodopsin reveals the pattern of helix movement due to activation. Proc. Natl. Acad. Sci. USA *105*, 7439–7444. https://doi.org/10.1073/pnas.0802515105.
19. Zhou, Q., Yang, D., Wu, M., Guo, Y., Guo, W., Zhong, L., Cai, X., Dai, A., Jang, W., Shakhnovich, E.I., et al. (2019). Common activation mechanism of class A GPCRs. Elife *8*, e50279. https://doi.org/10.7554/eLife.50279.
20. Fleetwood, O., Matricon, P., Carlsson, J., and Delemotte, L. (2020). Energy Landscapes Reveal Agonist Control of G Protein-Coupled Receptor Activation via Microswitches. Biochemistry *59*, 880–891. https://doi.org/10.1021/acs.biochem.9b00842.
21. Lee, J., Robinson, M.E., Ma, N., Artadji, D., Ahmed, M.A., Xiao, G., Sadras, T., Deb, G., Winchester, J., Cosgun, K.N., et al. (2020). IFITM3 functions as a PIP3 scaffold to amplify PI3K signalling in B cells. Nature *588*, 491–497. https://doi.org/10.1038/s41586-020-2884-6.
22. Koldsø, H., and Sansom, M.S.P. (2015). Organization and Dynamics of Receptor Proteins in a Plasma Membrane. J. Am. Chem. Soc. *137*, 14694–14704. https://doi.org/10.1021/jacs.5b08048.
23. Shorthouse, D., Hedger, G., Koldsø, H., and Sansom, M.S.P. (2016). Molecular simulations of glycolipids: Towards mammalian cell membrane models. Biochimie *120*, 105–109. https://doi.org/10.1016/j.biochi.2015.09.033.
24. Stansfeld, P.J., Hopkinson, R., Ashcroft, F.M., and Sansom, M.S.P. (2009). PIP2-binding site in Kir channels: Definition by multiscale biomolecular simulations. Biochemistry *48*, 10926–10933. https://doi.org/10.1021/bi9013193.
25. Tzortzini, E., and Kolocouris, A. (2023). Molecular Biophysics of Class A G Protein Coupled Receptors–Lipids Interactome at a Glance—Highlights from the A2A Adenosine Receptor. Biomolecules *13*, 957. https://doi.org/10.3390/biom13060957.
26. Bokoch, M.P., Zou, Y., Rasmussen, S.G.F., Liu, C.W., Nygaard, R., Rosenbaum, D.M., Fung, J.J., Choi, H.-J., Thian, F.S., Kobilka, T.S., et al. (2010). Ligand-specific regulation of the extracellular surface of a G-protein-coupled receptor. Nature *463*, 108–112. https://doi.org/10.1038/nature08650.
27. Ansell, T.B., Song, W., and Sansom, M.S.P. (2020). The Glycosphingolipid GM3 Modulates Conformational Dynamics of the Glucagon Receptor. Biophys. J. *119*, 300–313. https://doi.org/10.1016/j.bpj.2020.06.009.
28. Moukhametzianov, R., Warne, T., Edwards, P.C., Serrano-Vega, M.J., Leslie, A.G.W., Tate, C.G., and Schertler, G.F.X. (2011). Two distinct conformations of helix 6 observed in antagonist-bound structures of a β_1 -adrenergic receptor. Proc. Natl. Acad. Sci. USA *108*, 8228–8232. https://doi.org/10.1073/pnas.1100185108.
29. Liu, X., Xu, X., Hilger, D., Aschauer, P., Tiemann, J.K.S., Du, Y., Liu, H., Hirata, K., Sun, X., Guixà-González, R., et al. (2019). Structural Insights into the Process of GPCR-G Protein Complex Formation. Cell *177*, 1243–1251.e12. https://doi.org/10.1016/j.cell.2019.04.021.
30. Waskom, M. (2021). seaborn: statistical data visualization. J. Open Source Softw. *6*, 3021. https://doi.org/10.21105/joss.03021.
31. Michaud-Agrawal, N., Denning, E.J., Woolf, T.B., and Beckstein, O. (2011). MDAnalysis: A toolkit for the analysis of molecular dynamics simulations. J. Comput. Chem. *32*, 2319–2327. https://doi.org/10.1002/jcc.21787.
32. Berendsen, H.J.C., van der Spoel, D., and van Drunen, R. (1995). GROMACS: A message-passing parallel molecular dynamics implementation. Comput. Phys. Commun *91*, 43–56. https://doi.org/10.1016/0010-4655(95)00042-E.
33. Humphrey, W., Dalke, A., and Schulten, K. (1996). VMD: Visual molecular dynamics. J. Mol. Graph. *14*. 33-8–27-8. https://doi.org/10.1016/0263-7855(96)00018-5.

STAR★METHODS

KEY RESOURCES TABLE

REAGENT or RESOURCE	SOURCE	IDENTIFIER
Deposited data		
MD simulation trajectories	GPCRmd.org	1247
Software and algorithms		
GROMACS	www.gromacs.org	2021.4
VMD	https://www.ks.uiuc.edu/	1.9.4
MDAnalysis	https://www.mdanalysis.org/	2.5.0

RESOURCE AVAILABILITY

Lead contact

Further information and requests for resources should be directed to and will be fulfilled by the lead contact, Nagarajan Vaidehi (NVaidehi@coh.org).

Materials availability

This study does not generate any new unique materials.

Data and code availability

Data: all MD trajectories has been deposited to GPCRmd.org database under the dynamic ID 1247. These trajectories are publicly accessible.

Code: This study does not generate new code.

Any additional information required to reproduce the data reported in this study is available from the lead contact upon request.

METHOD DETAILS

MD simulations trajectories preparation

In our previous study,[14] we performed 22 μs of MD simulations to sampling the conformational heterogeneity of the full length ICL3 in β2AR. The absence of ICL3 in any resolved crystal or cryo-EM structures necessitated the use of computational modeling to construct the ICL3 loop. We generated four models of β2AR incorporating ICL3 (Figure S5; Table S1). Model A was a homology model of β2AR derived using the turkey β1AR inactive state structure (PDB: 2YCX),[28] including the ICL3 loop. For Model B, the intermediate state crystal structure (PDB: 6E67)[29] served as the template, with the entire ICL3 loop modeled to mirror the template structure. In Model C, while also using the intermediate state structure (PDB: 6E67)[29] as the foundation, we constructed the C-terminal portion of ICL3 as an alpha-helix and the remaining segment as a random coil. Model D, based on the same intermediate structure (PDB: 6E67),[29] features the ICL3 cap as an alpha-helix, with the rest of the loop modeled as a random coil. Details of the MD simulations are in ref.[14]

To streamline the trajectory data for subsequent analysis, our strategy is two-fold. Firstly, we seek to condense the expansive 22-millisecond trajectory, which is currently too extensive and may introduce unnecessary variability into our findings. To mitigate this and assure the integrity of our results, we implemented principal component analysis (PCA) on the root-mean-square deviation (RMSD) of the GPCR backbone. This technique allowed us to organize the trajectory into a number of distinct clusters. Our second aim is to draw a connection between these representative structures of the clusters and specific functional states that define GPCR activity. This will enable us to elucidate the influence of varying ICL3 conformations on the regulation of GPCR activity. The method employed in both steps will be elaborated in the following section.

Principal component analysis on GPCR backbone and acquire sub cluster trajectories

We utilized the 22 μs simulation trajectory from our prior research[14] and conducted a PCA based on their backbone RMSD. Subsequently, we projected the first two principal components (PC1 and PC2) onto an X-Y plane and established the population density contour map by using Seaborn KDE plot (Figure 1A).[30] To effectively group the sample points into distinct sub-states, we employed Kmeans clustering based on the PC1 and PC2 values. We iteratively set n_clusters from 2 to 20 and computed both the Silhouette score and the Davies-Bouldin index for each iteration. The results, as depicted in Figures S1A and S1B, indicate that a n_clusters value of 12 yields a high Silhouette score and a low Davies-Bouldin index. Consequently, we determined that n_clusters=12 is the optimal parameter for this clustering analysis.

After determining the 12 clusters, we assessed the population density by categorizing all data points into a 35x35 bins grid based on their PC1 and PC2 values. Within each of the 12 clusters, we identified the bin with the greatest population density. Only the frames from these

high-density bins were selected for subsequent analysis. Among the 12 identified clusters (Figure S1C), clusters 2 and 4 have sparse sampling points and do not display any global population density maximum as illustrated in Figure 1A. Consequently, we chose to exclude these two clusters and directed our attention solely to the remaining 10 clusters. From each of the 10 clusters, we then selected a subset of conformations that are within 10% when sorted by RMSD to the centroid of each cluster. This smaller conformational ensemble has been used for all subsequent analyses. The representative structures of each cluster are displayed as three-dimensional configurations in Figure 1A.

Distance measurement and hierarchical clustering

The distance measurements were conducted using the MDAnalysis distance module.[31] Specifically, the distance between residues 3.50-6.34 was determined between the Ca atoms of residue 131 and 272, in line with the BW numbering table provided by GPCRdb.org. The TM7-ICL3 cap distance was gauged as the minimum distance from R328 on TM7, to the center of mass (CoM) of residues 259 to 266 in ICL3. Hierarchical clustering was executed on the distances of 3.50-6.34 and the TM7-ICL3 cap from the 10 clusters, employing the single linkage method available in the scipy.cluster.hierarchy module. The D192-K305 distance was measured as the minimum distance between residue 192 and residue 305.

Contact analysis

In this study, all contact analyses were carried out using get_contact (get_contact.io). For Figure 2B, residues from ICL1, ICL2, and ICL3 were selected based on the BW table on GPCRdb.com. For Figure 2C, ICL3 residues and all PIP2 molecules present in the MD simulation were chosen. Meanwhile, for Figure 3I, residues from ECL2 and ECL3 as well as all GM3 molecules in the MD simulation were selected. The contact calculations were executed using the default parameters of get_contact. All types of contacts, such as van der Waals contacts, hydrogen bond contacts, and π-π contacts, were factored into the calculations.

Projecting lipid/GPCR onto X-Y plane

To generate lipid distribution contour maps as depicted in Figures 2A and 3G, several procedures were executed. Firstly, the protein structures were aligned using their Ca atoms. Next, the CoM for both the seven TM regions and the head groups of the targeted lipids, PIP2 and GM3, was determined. The TM region range was defined based on the BW numbering table from GPCRdb.com. To define the orientation of the GPCR, the average X and Y coordinates of the seven TMs CoM were projected onto the membrane X-Y plane. Additionally, the X and Y coordinates of each lipid molecule that consistently interacted (>20% simulation time) with either the intracellular loops (ICLs) or extracellular loops (ECLs) were also projected onto this plane. Through these processes, the spatial distribution and orientation of lipids relative to the GPCR became visible, providing a detailed insight into their interactions and placement.

Interaction interface area calculation

We employed the FreeSASA python module (www.freesasa.github.io), to compute the interaction interface area. Initially, we determined the total solvent-accessible surface area (SASA) for either ICL3 or ECL2 and all lipids within the MD simulation. Subsequently, the SASA was calculated separately for the ICL3 or ECL2 region and for all lipids. The interaction interface area is deduced by taking the sum of SASA for ICL3 or ECL2 and SASA for the lipids, and then subtracting the total SASA from this sum. We then computed the average interaction interface area for each of the 10 clusters independently. In Figures 2D and 3J, each cluster is represented by a single dot, indicating its average interaction interface area. A Mann-Whiteney U test (scipy.states.mannwhitneyu) was performed on the interaction interface area values to test the significancy. Given that the inactive state only has one cluster, we extracted average interaction interface area values from five distinct segments of inactive cluster, each consisting of consecutive frames of 20% of the total simulation length. This segmentation approach provides us sufficient data points for Mann-Whitney U test.

Calculation of membrane thickness

We have used Gromacs2022.1 for calculating membrane thickness for the membrane bilayer that is close to the receptor. Using gmx select command we have identified lipid molecules within 5Å radius of the receptor. Lipids for selection were defined as following: top leaflet: (name P or name O1) and (z > 5.5) and within 0.5 of group "Protein", bottom leaflet: (name P) and (z < 5.5) and within 0.5 of group "Protein". Then, distances between centers of mass of selected top and bottom leaflet lipids were calculated using gmx distance module.[32]

Radial pair distribution function G(r) calculation

The radial pair distribution function, denoted as G(r), was determined with the help of the VMD G(r) module.[31,33] Using the center of mass (CoM) of the entire GPCR as the central reference, we adopted a bin size of 0.5 Å for the radial pair. The calculation for G(r) spanned from 0 to 30 Å, and this was executed for all ten lipid types.

Ligand RMSD calculation

The ligand RMSD was calculated by using MDAnalysis.rms module.[31] We first align the protein by Ca atoms of TM region, using the initial model as reference. Then we calculate the RMSD of ligand per frame. All RMSD values of each state, after combining the corresponding clusters, were plotted in bar graph form in Figure 3C.

QUANTIFICATION AND STATISTICAL ANALYSIS

All statistical analyses were performed using Mann-Whiteney U test from scipy.states.mannwhitneyu, the p values were calculated using the default parameters.